An Improved Direct Decoupled Power Control of Doubly Fed Induction Machine Without Rotor Position Sensor and With Robustness to Parameter Variation

Navid Amiri, *Student Member, IEEE*, Seyed M. Madani, *Member, IEEE*, Thomas A. Lipo, *Life Fellow, IEEE*, and Hossein Abootorabi Zarchi

***Abstract*—In this paper, coupling between active and reactive powers in conventional direct power control (DPC) strategies is analyzed and a new direct DPC method for doubly fed induction machine without rotor position sensors is presented. Coupling analysis is done on an improved DPC strategy with rotor flux controllers in the stator reference frame. The presented control strategy is done by controlling the rotor flux in the grid flux reference frame. The rotor flux command is calculated using a predicted stator flux, the stator current command, and the stator resistance. Moreover, the rotor position is estimated by comparing measured and estimated values of the rotor current. Furthermore, to reduce the method's sensitivity to the parameter inaccuracies, the mutual inductance of the machine is updated during the machine operation by the error between the magnitudes of the measured and estimated values of the rotor current.**

***Index Terms*—Component, direct decoupled power control (DDPC), direct power control (DPC), doubly fed induction generator (DFIG), doubly fed induction machine (DFIM), model reference adaptive system (MRAS), sensorless.**

NOMENCLATURE

Ψ_s, Ψ_r	Stator and rotor flux linkage, vectors.
V_s, V_r	Stator and rotor voltage vectors.
I_s, I_r	Stator and rotor current vectors.
ω_1, ω_r, ω_{slip}	Synchronous, mechanical, and slip speeds.
R_s, R_r	Stator and rotor resistance.
L_{ls}, L_{lr}	Stator and rotor leakage inductance.
L_m	Machine mutual inductance.

Manuscript received November 17, 2011; revised March 10, 2012 and June 8, 2012; accepted July 9, 2012. Paper no. TEC-00614-2011.

N. Amiri is with the Department of Electrical and Computer Engineering, Isfahan University of Technology, Isfahan, Iran (e-mail: n.amiri@ec.iut.ac.ir).

S. M. Madani is with the Department of Electrical Engineering, University of Isfahan, Isfahan, Iran (e-mail: madani@cc.iut.ac.ir).

T. A. Lipo is with the Department of Electrical and Computer Engineering, University of Wisconsin-Madison, Madison, WI 53806 USA (e-mail: thomas.lipo1@gmail.com).

H. A. Zarchi is with the Department of Electrical Engineering, Ferdowsi University of Mashhad, Mashhad, Iran (e-mail: hazarchi@gmail.com).

Color versions of one or more of the figures in this paper are available online at http://ieeexplore.ieee.org.

Digital Object Identifier 10.1109/TEC.2012.2209889

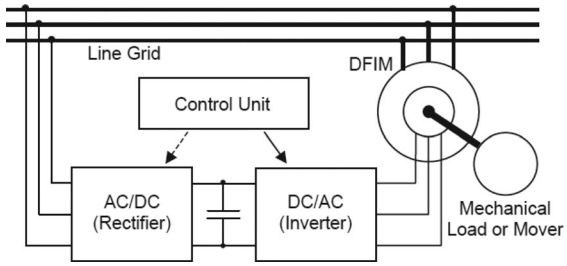

Fig. 1. Hardware setup for controlling a DFIM.

I. INTRODUCTION

In recent years, using renewable energy sources instead of the fossil fuel is constantly increasing. Most of the renewable energy sources come from natural events, which mostly have random characteristics. Wind energy as one of the natural renewable energy sources is used to generate power through wind turbines connected to an electric generator. Because of the randomness of wind speed in different areas, a flexible electric generation system is required to maintain constant frequency voltage and stable power. The doubly fed induction generator (DFIG) has characteristics which makes it a very good solution for wind generation application. The DFIG ability to operate in a rather large margin ($\pm 30\%$) around the synchronous frequency satisfies the requirements for a good wind generation system. First power control scheme for doubly fed induction machine (DFIM) was presented in 1983 which uses a cycloconverter to feed the rotor in order to control the stator power [1]. In the recent common configuration as shown in Fig. 1, the machine stator is directly connected to the grid and the rotor is fed by a three phase inverter at its rated power.

Vector control (VC) is commonly applied on DFIG using either flux-oriented [2], [3] or stator-voltage-oriented methods [4], [5]. In these methods, the stator flux and mechanical torque (or the stator power components) are assumed to be decoupled and controlled by the rotor current components along the real and imaginary axes of stator flux reference frame.

An alternative control method is the direct torque control (DTC) method which was first introduced for induction machines in [6] and [7] and quickly became a very good alternative to the commonly used VC methods. In the DTC method, the electromagnetic torque is instantaneously controlled based on

a predefined voltage vector lookup table in order to control the electromagnetic torque. However, the faster transient response compared to the conventional VC comes at the cost of inconstant switching frequency and higher torque ripple [8]. Work has been done by the researchers to address the problems of DTC by using space vector pulse width modulation (SVPWM) control technique for the inverter instead of switching tables to reduce torque ripple [9]–[11].

The direct power control (DPC) is established upon the principles of the DTC which directly controls the machine power. The DPC method uses switching tables to apply proper values of the rotor voltage components [12], [13]. To solve the inconstant switching frequency and the stator power components ripple, the SVPWM method is proposed to feed the rotor [14], [15]. Improvement of the DPC method proposes predictive power models, which allows the method to calculate the rotor voltage directly from the power components, and increase the power quality delivered by the generator [16], [17]. Further research is done on applying high performance nonlinear controllers like sliding mode controllers [18] and model based predictive controllers [19]. In [20] and [21], an improved DPC method with a high performance under unbalanced grid conditions is introduced. To increase system reliability, several sensorless control methods have been developed [22]. A complete overview including introduction, modeling, and different control methods for DFIMs is presented in [23]. In most DPC strategies, the stator resistance is neglected, and therefore, the stator flux magnitude is considered to be constant. However, the existence of the stator resistance causes the stator flux to be affected by the changes in stator current or power flow. This results in variations in stator flux, which is the reference frame in most of the introduced methods, and causes coupling between the stator power components. This problem can be solved by compensating the effect of stator resistance voltage drop on rotor flux (or voltage) control loop. Moreover, the grid flux is chosen as the reference frame, in which the stator voltage vector is always at 90° ahead of the grid flux vector. This results in the stator power to be only affected by the stator current components. Therefore, the rotor flux can be calculated and controlled in this reference frame in a way to decouple the stator active and reactive power controllers.

For accurate operation of the position/speed sensorless control, the machine quantities such as rotor position, stator, and rotor flux vectors must be estimated. These estimations require the exact values of the machine voltages, currents, and parameters. In case of a DFIM, both the stator and rotor currents and voltages can be measured. This is an important advantage of DFIM over other types of electrical machines. Having these extra measurable quantities causes the estimation process to be robust to the machine parameters inaccuracies. Moreover, the estimated parameters of the machine can be enhanced during the control process, by using the error between measured and estimated quantities. As an example, the measured and estimated rotor current vector, consisting of magnitude and angle, can be used to enhance the rotor position estimation. The following sections will first give a quick introduction to the DFIM followed by an improved conventional DPC method [24]. Then, the coupling between the active and reactive powers due to stator resistance will be discussed. Subsequently, the proposed direct decoupled power control (DDPC) method is explained, and finally, sensorless control and parameter correction strategy are presented.

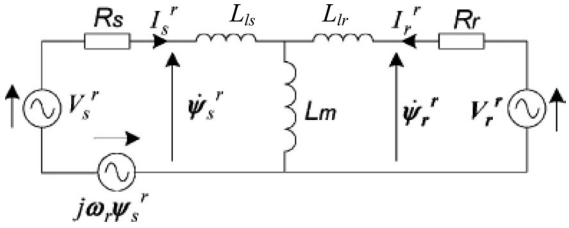

Fig. 2. Equivalent Circuit of DFIM in the rotor frame.

II. DFIM

A. Model Equations

The equivalent circuit of the DFIM in the rotor reference frame is shown in Fig. 2.

According to Fig. 2, stator and rotor flux equations in the rotor reference frame can be written (the *r* superscript stands for rotor reference frame) as

$$\overrightarrow{\psi_s^r} = L_s\overrightarrow{I_s^r} + L_m\overrightarrow{I_r^r} \tag{1}$$

$$\overrightarrow{\psi_r^r} = L_m\overrightarrow{I_s^r} + L_r\overrightarrow{I_r^r} \tag{2}$$

where $L_s = \mathrm{L}_m + \mathrm{L}_{ls}$ and $L_r = \mathrm{L}_m + \mathrm{L}_{lr}$. For the stator and rotor voltages, we have

$$\overrightarrow{V_s^r} = R_s\overrightarrow{I_s^r} + \frac{d\overrightarrow{\psi_s^r}}{dt} + j\omega_r\overrightarrow{\psi_s^r} \tag{3}$$

$$\overrightarrow{V_r^r} = R_r\overrightarrow{I_r^r} + \frac{d\overrightarrow{\psi_r^r}}{dt}. \tag{4}$$

According to (1) and (2), stator current can be written as

$$\overrightarrow{I_s^r} = \frac{L_r\overrightarrow{\psi_s^r} - L_m\overrightarrow{\psi_r^r}}{L_sL_r - L_m^2} = \frac{\overrightarrow{\psi_s^r}}{\sigma L_s} - \frac{L_m\overrightarrow{\psi_r^r}}{\sigma L_sL_r} \tag{5}$$

where $\sigma = (L_sL_r - L_m^2)/L_sL_r$. According to (3) and by neglecting the stator resistance, the stator active power can be written as

$$P_s = \frac{3}{2}\overrightarrow{V_s^r}\cdot\overrightarrow{I_s^r} = \frac{3}{2}(\frac{d\overrightarrow{\psi_s^r}}{dt} + j\omega_r\overrightarrow{\psi_s^r})\cdot\overrightarrow{I_s^r}. \tag{6}$$

In the same way, the stator reactive power equation is

$$Q_s = \frac{3}{2}|\overrightarrow{V_s^r}\times\overrightarrow{I_s^r}| = \frac{3}{2}\left|\left(\frac{d\overrightarrow{\psi_s^r}}{dt} + j\omega_r\overrightarrow{\psi_s^r}\right)\times\overrightarrow{I_s^r}\right|. \tag{7}$$

The stator flux in the stationary stator frame can be obtained using the following equation (the *s* superscript stands for stator reference frame):

$$\overrightarrow{\psi_s^s} = \int(\overrightarrow{V_s^s} - R_s\overrightarrow{I_s^s})dt. \tag{8}$$

Because the resistive voltage drop on the stator windings has a small effect on the stator flux magnitude, the stator flux

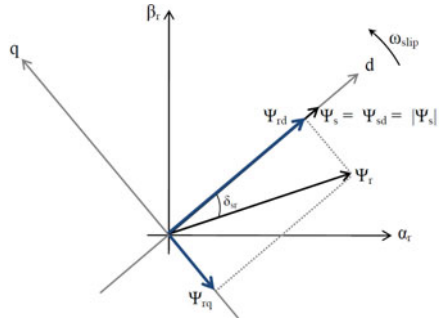

Fig. 3. Stator and rotor fluxes in the rotor reference frame (α_r –β_r).

magnitude can be considered constant in both stationary and rotor reference frames:

$$|\overrightarrow{\psi_s^s}| = |\overrightarrow{\psi_s^r}| = \left| \int \overrightarrow{V_s^s} dt \right| = \text{constant}. \tag{9}$$

Using (5)–(7) and considering the constant magnitude of the stator flux vector from (9), the stator active and reactive powers can be rewritten as

$$P_s = -\frac{3}{2}\frac{L_m}{\sigma L_s L_r}\omega_1 |\overrightarrow{\psi_s^r}||\overrightarrow{\psi_r^r}| \sin\delta_{sr} \tag{10}$$

$$Q_s = \frac{3}{2}\frac{\omega_1}{\sigma L_s}\left|\overrightarrow{\psi_s^r}\right|\left(\frac{L_m}{L_r}\left|\overrightarrow{\psi_r^r}\right|\cos\delta_{sr} - \left|\overrightarrow{\psi_s^r}\right|\right) \tag{11}$$

where δ_{sr} is the angle between the stator and rotor flux vectors.

III. DPC OF DFIM

A. Control Strategy

According to the active and reactive powers (10) and (11), power can be controlled by controlling the magnitude and relative angle of either the rotor or stator fluxes. In common practice, the DFIM stator is directly connected to the grid and its flux magnitude and angle are determined by the stator voltage and current. Therefore, direct control of the machine active and reactive powers can be achieved, by applying the accurate rotor flux magnitude and angle (relative to the stator flux). As mentioned earlier, the stator flux magnitude is considered to be constant due to negligible stator resistance effect.

It can be seen from (10) and (11) that controlling the active and reactive powers of the machine's stator has direct linear relation with the rotor flux components (along the quadrature and direct axis of the stator flux). Therefore, it is appropriate to use the stator flux vector as the reference frame for the control process. On the other hand, eventually the rotor voltages and currents must be calculated and applied in the rotor reference frame.

Fig. 3 shows the stator and rotor flux vectors in the rotor reference frame.

According to (10), (11), and (4) active and reactive powers and rotor voltage equations can be written as follows:

$$P_s = \frac{3}{2}\frac{L_m}{\sigma L_s L_r}\omega_1 \psi_{sd}\psi_{rq} \tag{12}$$

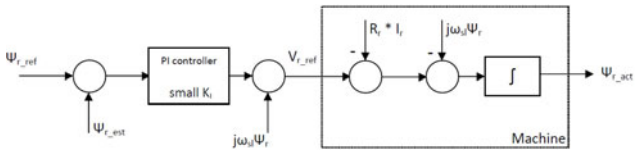

Fig. 4. Rotor flux controller.

$$Q_s = \frac{3}{2}\frac{\omega_1}{\sigma L_s}\psi_{sd}\left(\frac{L_m}{L_r}\psi_{rd} - \psi_{sd}\right) \tag{13}$$

$$V_{rd} = R_r I_{rd} + \frac{d\psi_{rd}}{dt} + \omega_{\text{slip}}\psi_{rq} \tag{14}$$

$$V_{rq} = R_r I_{rq} + \frac{d\psi_{rq}}{dt} - \omega_{\text{slip}}\psi_{rd}. \tag{15}$$

By neglecting the rotor resistance in (14) and (15), one has

$$\frac{d\psi_{rd}}{dt} = V_{rd} - \omega_{\text{slip}}\psi_{rq} \tag{16}$$

$$\frac{d\psi_{rq}}{dt} = V_{rq} + \omega_{\text{slip}}\psi_{rd}. \tag{17}$$

It can be seen that controlling the active and reactive powers can be achieved by having the accurate rotor flux along the *q*- and *d*-axis, respectively. One can conclude from (16) and (17) that controlling the rotor flux components along the *dq*-axis can be done by applying the correct rotor voltages in the corresponding axis. Since there is a rotational voltage caused by the slip frequency, the motion induced rotor voltages are feed forwarded to decouple the rotor flux control loops. One can see from (16) and (17) that the actual rotor flux is calculated by integrating the applied rotor voltage. In other words, there is an integrator in the plant (i.e., the machine block diagram). Therefore, the rotor flux controller just need a proportional P controller to achieve zero steady-state error for step input, and an integrator is not needed. However, a small integral gain is used to compensate the effect of rotor resistance and machine parameters inaccuracies. The rotor flux control loop is shown in Fig. 4.

IV. COUPLING BETWEEN ACTIVE AND REACTIVE POWERS

A. Analyzing the Effect of Stator Power and Current on Stator Flux Frame

The previous section shows that the active and reactive powers of the stator can be controlled by controlling the q and d components of the rotor flux along the stator flux vector. According to (12) and (13), the power control can be decoupled when the stator flux phasor is considered to be constant and unaffected by the changes in the machine stator power. However, according to (8), the stator flux is affected by the changes in stator current due to the existence of stator resistance, which rotates the reference frame.

To analyze the coupling between the stator power components control loops, it is necessary to analyze the impact of stator current on the stator flux. For the sake of simplicity, this analysis is done in the stator voltage reference frame ($V_{sQ} = |\vec{V}_s|$ and $V_{sD} = 0$). Therefore, the stator flux can be calculated using the

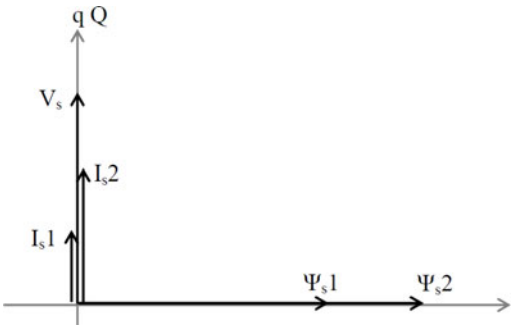

Fig. 5. Effects of the stator active power variations on the stator flux (zero reactive power).

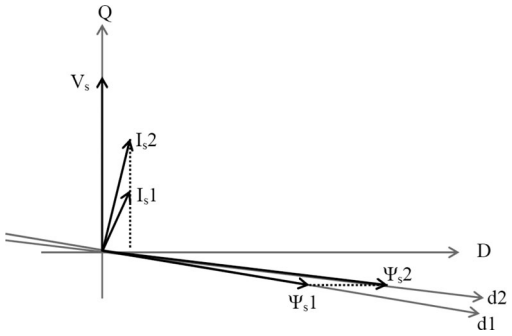

Fig. 6. Effects of the stator active power variations on the stator flux (nonzero reactive power).

following equations:

$$\dot{\psi}_{sD} = R_s I_{sD} + \omega_1 \psi_{sQ} \tag{18}$$

$$\dot{\psi}_{sQ} = V_{sQ} + R_s I_{sQ} - \omega_1 \psi_{sD}. \tag{19}$$

Considering the equations in a steady-state sinusoidal condition, the stator flux vector can be expressed as follows:

$$\overrightarrow{\psi_s} = \frac{R_s \overrightarrow{I_s}}{j\omega_1} + \frac{\overrightarrow{V_s}}{j\omega_1}. \tag{20}$$

It can be seen from (18)–(20) that both the magnitude and angle of the stator flux vector are affected by the stator current variations. The stator current can be divided into active and reactive components, by its projection in direction and quadrant to the stator voltage. Then, the effect of each current component on the stator flux can be analyzed.

1) Effect of stator current active component on stator flux:
According to (20), this effect is shown in Figs. 5 and 6.

Figs. 5 and 6 show that the active component of the stator current changes the magnitude of the stator flux vector without considerably affecting its angle.

1) Effect of stator current reactive component on stator flux:
According to (20), this effect is shown in Fig. 7.

Fig. 7 shows that the reactive component of the stator current changes the angle of the stator flux without considerably affecting its magnitude.

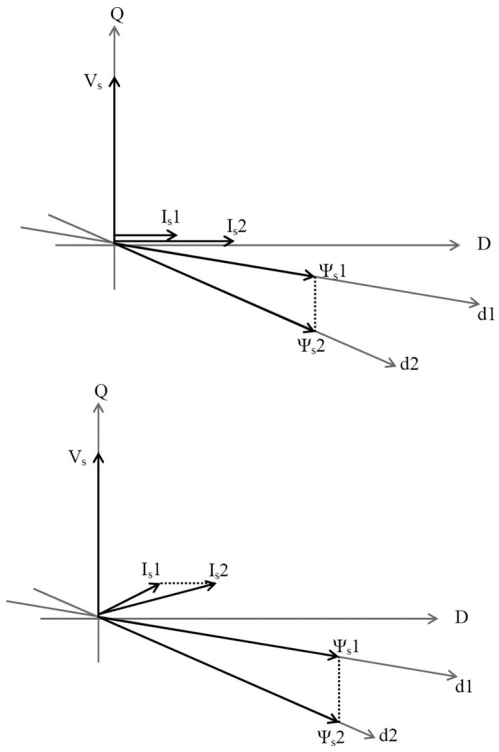

Fig. 7. Effects of the stator reactive power variations on the stator flux (a) zero (b) nonzero active power.

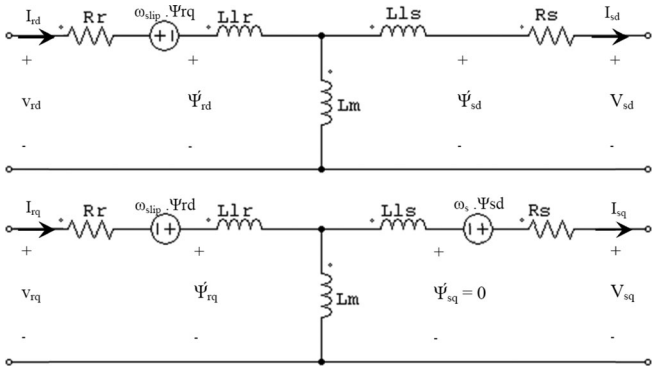

Fig. 8. DFIM equivalent circuit in the stator flux reference frame.

B. Analyzing the Coupling Between Stator Active and Reactive Powers in Conventional DPC Strategies

In conventional DPC strategies, stator active and reactive powers are controlled by controlling the rotor flux q and d components along the stator flux vector, respectively. However, because of stator resistance voltage drop effect, the stator flux is not constant and is affected by stator power variations as discussed in previous section. To find a solution for decoupling the power control loops, first, coupling between the stator power components control loops should be analyzed. Fig. 8 shows the equivalent circuit of a DFIM in stator flux reference frame.

According to the equivalent circuit in Fig. 8, the stator active and reactive powers can be calculated as

$$P_s = V_{sq} I_{sq} + V_{sd} I_{sd} \tag{21}$$

$$Q_s = V_{sq} I_{sd} + V_{sd} I_{sq}. \tag{22}$$

In (21) and (22), the stator voltage and current can be written in terms of stator and rotor flux according to the equivalent circuit of Fig. 2 (in which the rotor leakage inductance is neglected and therefore, $L_l = L_{ls}$).

$$V_{sd} = \dot{\psi}_{sd} - \frac{R_s}{L_l}(\psi_{rd} - \psi_{sd}) \tag{23}$$

$$V_{sq} = \omega_1 \psi_{sd} - \frac{R_s}{L_l}\psi_{rq} \tag{24}$$

$$I_{sd} = \frac{1}{L_l}(\psi_{rd} - \psi_{sd}) \tag{25}$$

$$I_{sq} = \frac{1}{L_l}\psi_{rq}. \tag{26}$$

By substituting the stator voltage and current from (23)–(26) into (21) and (22), the following equations can be written for the stator power components:

$$P = \frac{1}{L_l}\left[\psi_{rq}\left(\omega_1 \psi_{sd} - \frac{R_s}{L_l}\psi_{rq}\right) - \frac{R_s}{L_l}(\psi_{rd} - \psi_{sd})^2 + \dot{\psi}_{sd}(\psi_{rd} - \psi_{sd})\right] \tag{27}$$

$$Q = \frac{1}{L_l}\left[(\psi_{rd} - \psi_{sd})\left(-\frac{2R_s}{L_l}\psi_{rq} + \omega_1 \psi_{sd}\right) + \psi_{rq}\dot{\psi}_{sd}\right]. \tag{28}$$

Equations (27) and (28) show that due to stator resistance, each stator power components have nonlinear relation to both of the rotor flux components and cannot be controlled independently. Since the leakage inductance is small, the term (R_s/L_l) is not negligible.

Note that by letting $R_s = 0$ and considering the stator flux to be constant in (27) and (28), the power components equations will be the same, as mentioned in (12) and (13). This coupling between stator power control loops can also be verified using the machine's vector diagram during stator power commands. According to the equivalent circuit of the machine in Fig. 2, the stator current components can be written in terms of stator and rotor flux vectors as follows:

$$I_{sd} = \frac{\psi_{rd} - \psi_{sd}}{L_l} \tag{29}$$

$$I_{sq} = \frac{\psi_{rq}}{L_l}. \tag{30}$$

In conventional DPC of DFIM, the stator active and reactive powers are controlled using the *q* and *d* components of the rotor flux, respectively. Therefore, two vector diagrams can be shown for each stator power component command. (Note that the rotor leakage inductance is neglected in the following diagrams.)

1) Stator active power command:

According to (12), the stator active power command changes only the *q* component of the rotor flux command. Thus, using (27) and Fig. 7, the vector diagram of the process is shown in Fig. 9.

According to (12) and Fig. 9, changes in the *q* component of the rotor flux can change both the stator active and reactive power components due to the effect of stator resistance, which verifies the coupling between stator active and reactive power control loops. Fig. 9 shows the process of applying active power command while the reactive power control loop is open.

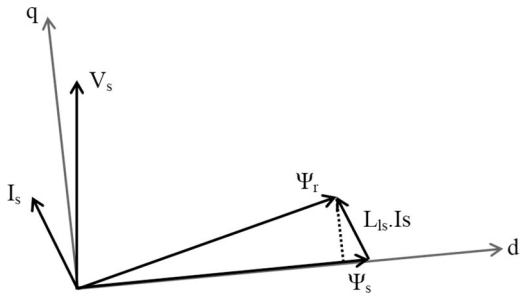

Fig. 9. Vector diagram of the DFIM after the stator active power command.

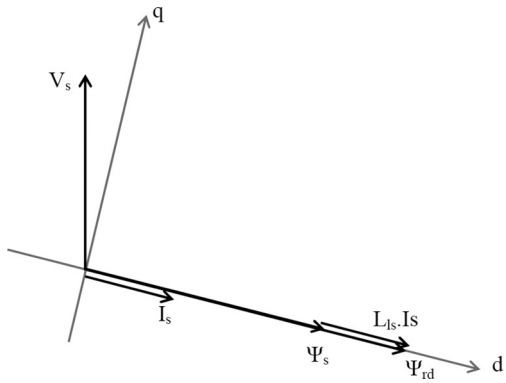

Fig. 10. Vector diagram of the DFIM after the stator reactive power command.

1) Stator reactive power command:

According to (13), the stator reactive power command affects only the *d* component of the rotor flux command. This procedure is depicted in Fig. 10 after stator reactive power command.

According to (13) and Fig. 10, an increase in the *d* component of the rotor flux initially causes the stator current to increase along the *d*-axis. However, because of the stator resistance effect, the *d* component of the stator current will create a negative amount of stator flux along the *q*-axis, which rotates the reference frame and creates coupling between active and reactive power control loops. Fig. 10 shows the process of applying a reactive power command while the active power controller loop is open. There are two main reasons for the coupling between the stator power components in this control strategy: 1) existence of stator resistance which causes the stator flux magnitude and angle to be affected by stator power variations; and 2) the stator voltage and current vectors are changed due to the rotation of the stator flux reference frame. In the next section, a solution for these problems is proposed.

V. DDPC OF DFIM

A. DFIM Model in Grid Flux Reference Frame

As shown in the previous section, the stator flux reference frame is affected by changes in stator power which consequently changes *dq* components of the stator voltage and current. Such a reference frame deviation disturbs the decoupled properties of

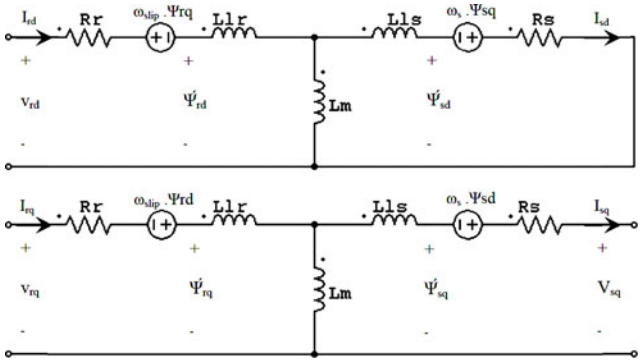

Fig. 11. *dq* equivalent circuit of DFIM in the grid flux reference.

dq control loops. To solve this problem, one needs a reference frame to be stationary relative to either the stator voltage or current vectors. To achieve this goal, the grid flux reference frame is chosen. In this reference frame, the grid flux is calculated by the following equation:

$$\overrightarrow{\psi_g^s} = \int \overrightarrow{V_s^s} dt. \tag{31}$$

In (31), the stator voltage vector is equal to the grid voltage and is totally independent of the stator current vector. Moreover, the stator voltage vector is always on the q-axis

$$V_{sq} = |\overrightarrow{V}_s|, \quad V_{sd} = 0. \tag{32}$$

In this reference frame, the active and reactive power equations can be written as

$$P_s = V_{sq} I_{sq} \tag{33}$$

$$Q_s = V_{sq} I_{sd}. \tag{34}$$

Equations (33) and (34) show that the stator active and reactive power components can be controlled using q and d components of the stator current, respectively. To develop a control strategy, the model of the DFIM in the grid flux reference frame should be introduced. Fig. 11 shows the *dq* equivalent circuit of the machine in the grid flux reference frame.

According to Fig. 11, by neglecting the rotor leakage inductance ($L_l = L_{ls}$), the stator current components can be written as follows:

$$I_{sd} = \frac{\psi_{rd} - \psi_{sd}}{L_l} \tag{35}$$

$$I_{sq} = \frac{\psi_{rq} - \psi_{sq}}{L_l}. \tag{36}$$

B. DDPC of DFIM

According to the proposed control system in Section III, the power control is done by controlling the corresponding rotor flux components along the *d*- and *q*-axis. In Section IV, it is shown that the magnitude and angle of the stator flux vector change with the stator power variation. This causes both *d* and *q* components of the stator current vector to be affected by the *dq* rotor flux commands. To solve this problem, the accurate relation between rotor flux vector and stator current vector is

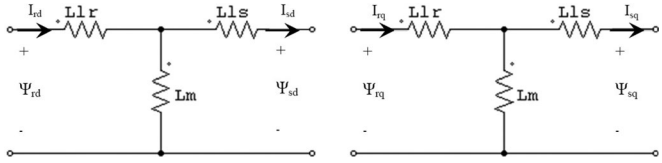

Fig. 12. Equivalent circuit of the machine from the stator and rotor flux viewpoint in the grid flux reference frame.

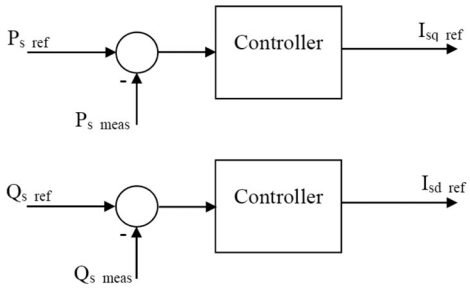

Fig. 13. Active and reactive power controllers.

necessary. Fig. 12 shows the machine equivalent circuit from the stator and rotor currents point of view.

By neglecting the rotor leakage inductance ($L_l = L_{ls}$), the rotor flux vector *dq* components can be written as follows:

$$\psi_{rd} = \psi_{sd} + L_l I_{sd} \tag{37}$$

$$\psi_{rq} = \psi_{sq} + L_l I_{sq}. \tag{38}$$

In (37) and (38), the stator flux vector *dq* components is a function of the stator current. Therefore, the rotor flux vector command can be obtained based on the stator current command as follows:

$$\overrightarrow{\psi_r} = f_{dq}(\overrightarrow{I_s}) + L_l \overrightarrow{I_s}. \tag{39}$$

Also, since stator active and reactive power components have linear relations with I_{sq} and I_{sd}, respectively, the stator current command can be obtained from the power controllers, as shown in Fig. 13.

To obtain the rotor flux vector commands, $f_{dq}(I_s)$ is defined as the predicted stator flux vector as a function of stator current vector command. It should be noted that the actual stator flux vector cannot be used in calculating the rotor flux vector command because the rotor flux cannot be controlled instantaneously. By applying the described rotor flux vector command, the active and reactive powers can be controlled decoupled from each other. Fig. 14 shows the vector diagram of the active power control of the machine.

Fig. 14 shows that after an increasing active power command, the old control only increases the q component of rotor flux command. However, the new method has also additional slight increase in the d component of that command to compensate the additional required stator flux. Therefore, by predicting this increase (in the stator flux component along the d-axis) and adding it to the new rotor flux command, the stator current can be kept on the q-axis and in phase with the stator voltage. Fig. 15 shows the same procedure during reactive power command in the proposed method, where the changes of the stator flux vector

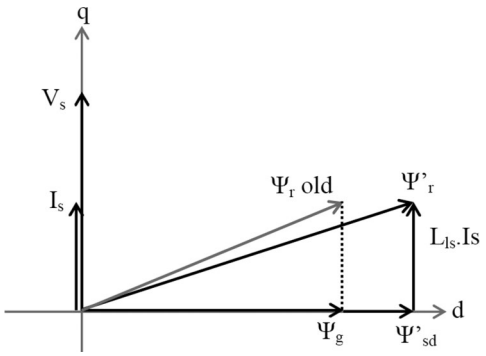

Fig. 14. Vector diagram of the DFIM rotor flux command after a step increase in the reference active power in the proposed strategy.

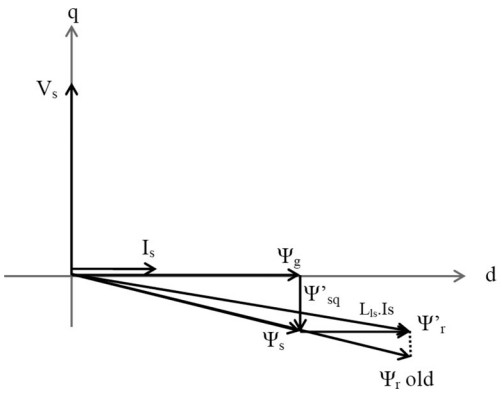

Fig. 15. Vector diagram of the DFIM rotor flux command after a step increase in the reference reactive power in the proposed strategy.

along the *q*-axis is compensated by the rotor flux additional *q* component command along with its normal command along the *d*-axis.

C. Calculating Stator Flux Command

There are two ways to calculate the stator flux command which are based on the equivalent circuit of the machine in either the grid flux reference frame or in stationary frame.

1) Calculating stator flux command in the grid flux frame:

Here, the stator flux vector is calculated in terms of stator voltage and current vectors as follows:

$$\psi_{sd} = \int (R_s I_{sd} - \omega_1 \psi_{sq}) dt \tag{40}$$

$$\psi_{sq} = \int (V_{sq} + R_s I_{sq} - \omega_1 \psi_{sd}) dt. \tag{41}$$

The block diagram of these calculations is shown in Fig. 16.

1) Calculating stator flux command in the stationary frame:

The stator flux command in the grid flux frame can be also calculated by transferring the stator currents to the stator stationary $\alpha\beta$ frame and then, using the following equation:

$$\overrightarrow{\psi}^*_{s\alpha\beta} = \int (\overrightarrow{V}_{s\alpha\beta} + R_s \overrightarrow{I}^*_{s\alpha\beta}) dt \tag{42}$$

where $\overrightarrow{I}^*_{s\alpha\beta}$ is the stator current command in the stator stationary frame. By transforming the $\Psi^*{}_{s\alpha\beta}$ back to the grid flux

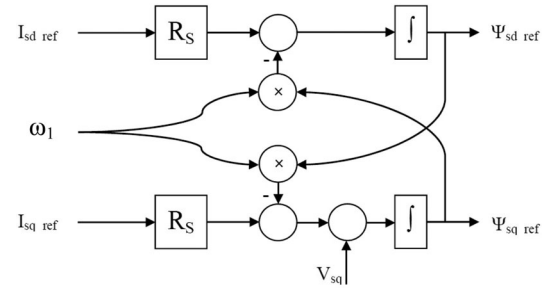

Fig. 16. Estimation of the reference stator flux vector using the equivalent circuit method.

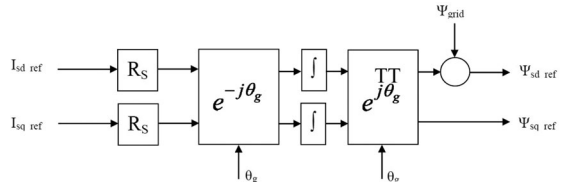

Fig. 17. Estimation of the reference stator flux vector using the stator stationary frame method.

frame, the reference stator flux in the *dq* frame can be obtained.

$$\psi^*_{sd} = \psi^*_{s\alpha} \cos\theta_g - \psi^*_{s\beta} \sin\theta_g \tag{43}$$

$$\psi^*_{sd} = \psi^*_{s\alpha} \cos\theta_g - \psi^*_{s\beta} \sin\theta_g \tag{44}$$

where θ_g is the grid flux vector angle in the stator stationary frame. Fig. 17 shows the block diagram of this calculation.

VI. Sensorless Operation and Parameter Correction

A. Sensorless Operation

Slip and rotor angle estimation is based on the difference of the same quantity in two different reference frames, which in this case is the rotor current. The rotor current in the rotor reference frame can be obtained by directly measuring the current at the rotor terminals. Since the rotor current oscillates with the slip frequency, the angle of the rotor measured current vector is an accurate estimation of the slip angle. On the other hand, the rotor current in the synchronous reference frame can also be calculated using the machine voltage and flux equations, which oscillates with the synchronous frequency. The difference between the rotor current angles in the rotor and synchronous reference frame will result in the (electrical) rotor angle, which is the mechanical rotor angle multiplied by motor pole pairs. This rotor angle can be used to transform any parameter from the synchronous frame to the rotor frame and vice versa. Therefore, by knowing the difference between the rotor current angle and the grid flux angle in the synchronous frame, one can allocate the grid flux angle, in the rotor frame. Fig. 18 shows the grid flux and rotor current in the rotor, stator, and stator flux reference frames.

The equation regarding the calculation of the slip and rotor angles is

$$\theta_{\text{slip}} = \theta_g = \theta^r_{\psi g} = \theta^s_{\psi g} - (\theta^s_{Ir} - \theta^r_{Ir}). \tag{45}$$

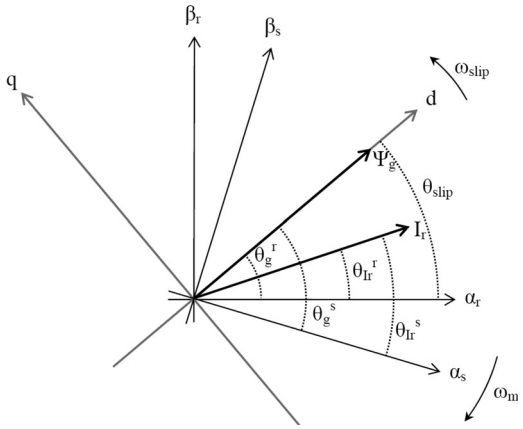

Fig. 18. Rotor current and Grid flux in both the stator and rotor reference frame.

In (45), the angle of the grid flux in the stator frame $\theta^s_{\psi g}$ can be calculated by the estimation of the grid flux in (31). Therefore, one has

$$\theta^s_{\psi g} = \tan^{-1}\left(\frac{\int V_s^{\beta s} dt}{\int V_s^{\alpha s} dt}\right). \tag{46}$$

Also, the angle of the rotor current in the stator reference frame is calculated by using the estimated rotor current in the following equation:

$$\overrightarrow{I}_r = \frac{\overrightarrow{\psi}_s - L_s \overrightarrow{I}_s}{L_m} \tag{47}$$

$$\theta^s_{Ir} = \tan^{-1}\left(\frac{\int (V_s^{\beta s} - R_s I_s^{\beta s})dt - L_s I_s^{\beta s}}{\int (V_s^{\alpha s} - R_s I_s^{\alpha s})dt - L_s I_s^{\alpha s}}\right) \tag{48}$$

where $V_{s\alpha\beta}$ and $I_{s\alpha\beta}$ are the measured stator voltage and current at the stator terminals.

Finally, the angle of the rotor current in the rotor frame can be directly calculated from the measured rotor currents at the rotor terminals

$$\theta^r_{Ir} = \tan^{-1}\frac{I_r^{\beta r}}{I_r^{\alpha r}}. \tag{49}$$

B. Parameter Correction

Obtaining the accurate rotor and slip angles relies on having the precise values of the machine's parameters. One of the most important parameters used in estimating the machine's flux and current vectors is the mutual inductance between the rotor and stator windings. Inaccuracies in this particular parameter will lead to wrong estimation of the rotor current and, therefore, inaccurate estimation of rotor and slip angles. To tackle this problem, a simple form of the model reference adaptive system (MRAS) is used, which is based on comparing a measured value with the estimated value of a same quantity of the system and use the error signal to correct specific parameters in the model. In this case, one has both the measured and estimated value of the rotor current. The difference between the angles of these two values is used to estimate the rotor angle. But according to (47), the difference between the amplitude of the measured and estimated value of the rotor current can be used to correct the value of L_m. Fig. 19 shows the diagram of the described method.

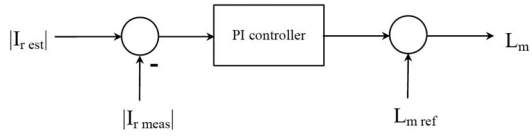

Fig. 19. MRAS loop for correcting the mutual inductance.

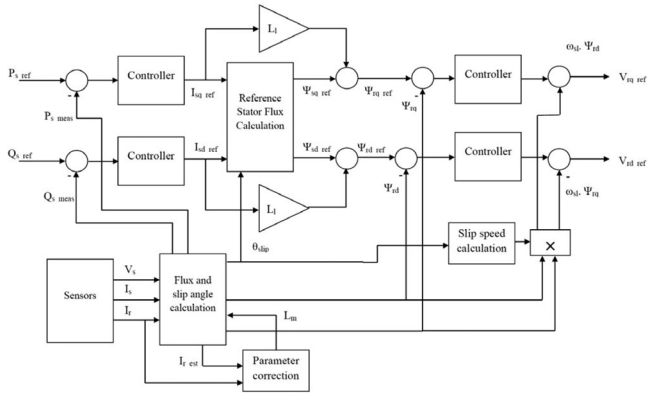

Fig. 20. Complete control diagram of the proposed decoupled DPC method.

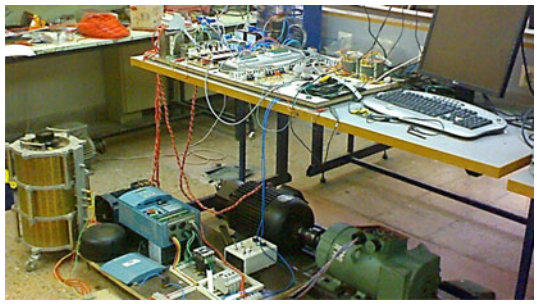

Fig. 21. Four-KW experimental setup.

To prevent the parameter correction loop dynamics from affecting the power control algorithm, a very small proportional gain is set in the applied PI controller.

C. Complete DDPC Block Diagram

The complete block diagram of the proposed method is shown in Fig. 20.

VII. Simulation and Experimental Results

The proposed method has been simulated on a 4-KW DFIM. The rotor windings are fed by a SVPWM controlled inverter, operating with the switching frequency of 10 KHz. The dc-link voltage has been set on 200 V and is kept constant by a grid-connected converter during the process. The control strategy is also applied to a DSP-based 4-KW experimental setup, showed in Fig. 21 to validate the simulation results. The machine parameters used in the simulation are given in Table I.

TABLE I
MACHINE PARAMETERS

Machine parameters	Parameter value
Nominal Power	4000 W
Nominal speed	1440 rpm
Mutual inductance	0.21 H
Stator leakage inductance	2.4 mH
Rotor leakage inductance	2.4 mH
Stator resistance	1 Ω
Rotor resistance	0.2 Ω
Pole Pairs	2

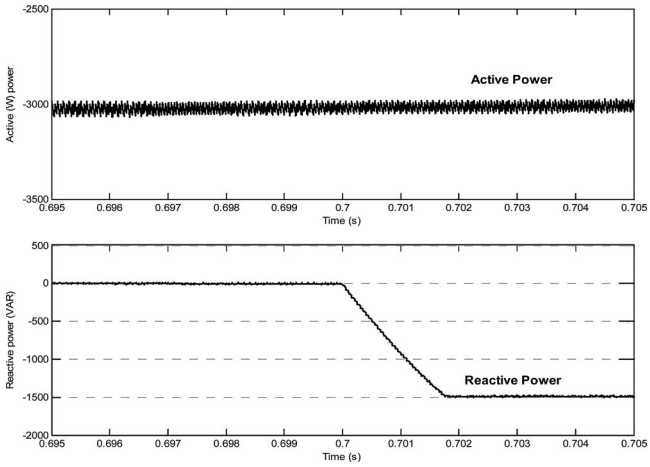

Fig. 22. Simulation result of the stator active (W) and reactive power (Var) during reactive power command using the proposed strategy.

The power controllers' constants are $K_p = 6$ and $K_I = 2$. The proportional gain of the flux controller is $K_p = 50$.

Fig. 22 shows the active power of the machine is unaffected by the fast response of the stator reactive power, which confirms the decoupling between active and reactive power control. To compare the proposed strategy and the conventional DPC, the simulation is done when the power controllers are open loop and the active power controller output is changed manually by a step function. The rotor flux vector and the stator power variations in the conventional DPC and the proposed DDPC are shown in Figs. 23–25 respectively.

Fig. 25 shows that the active and reactive powers are reasonably decoupled from each other in the proposed DDPC control process. Fig. 26 shows the estimated slip angle of the machine along with rotor speed variation.

Fig. 26 shows that the proposed sensorless strategy is able to accurately estimate the slip angle.

Fig. 27 shows that the proposed parameter correction loop is able to effectively compensate large machine parameter errors. Also because of the slow operation of the controller used in the loop, it has ignorable effect on the power control dynamics. In Fig. 28, difference between the calculated stator flux angle using the correct mutual inductance and the stator flux angle

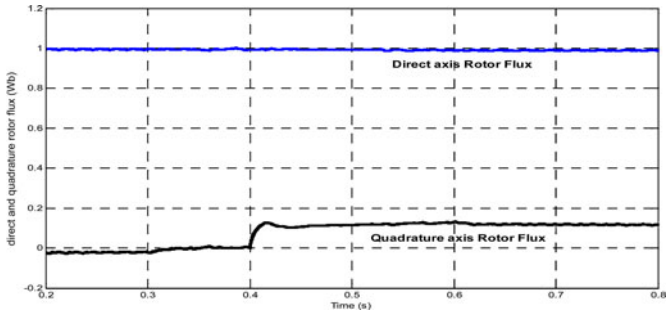

Fig. 23. Rotor flux vector of the DFIM during step change of the active power controller while the power controllers are open loop (conventional DPC).

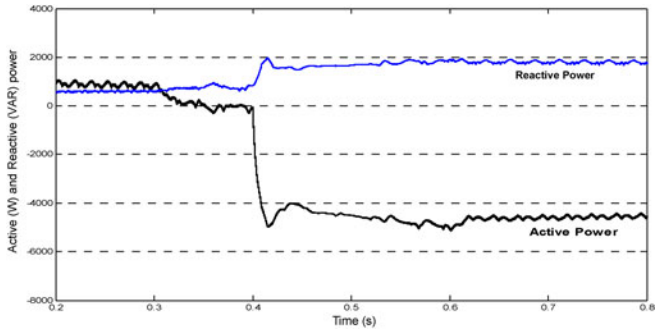

Fig. 24. Stator power variation of the DFIM during step change of the active power controller while the power controllers are open loop (conventional DPC).

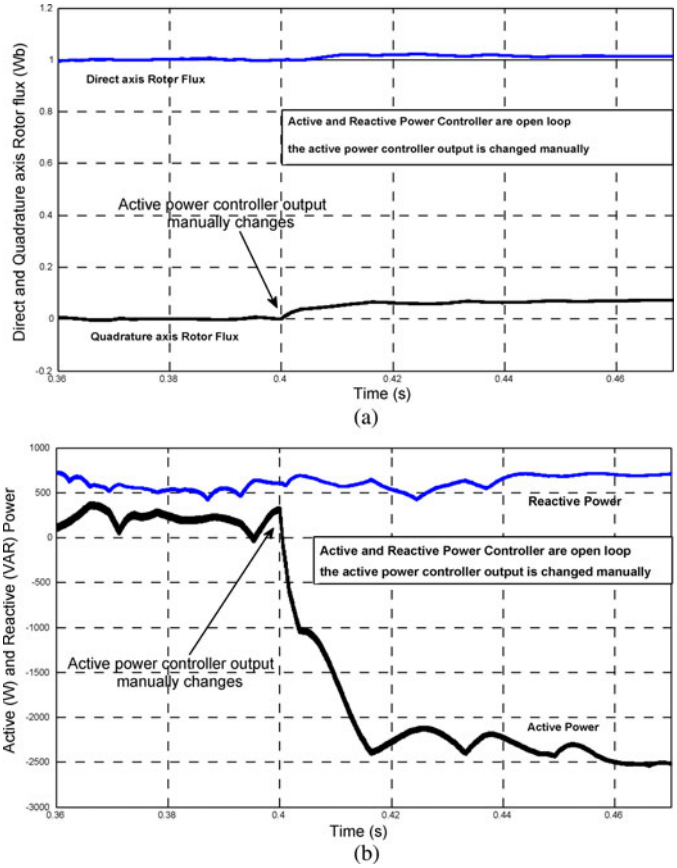

Fig. 25. (a) Rotor flux vector and (b) stator power variations of the DFIM during step change of the active power controller while the power controllers are open loop (proposed DDPC).

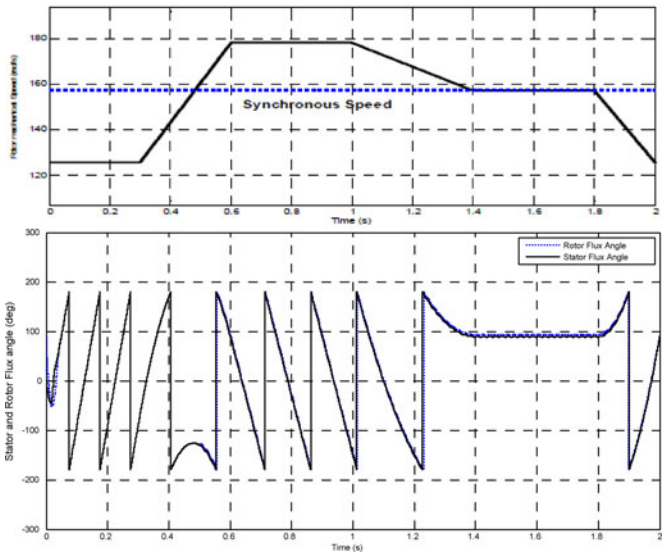

Fig. 26. Estimated slip angle (in degrees) of the machine according to the changes in the rotor speed.

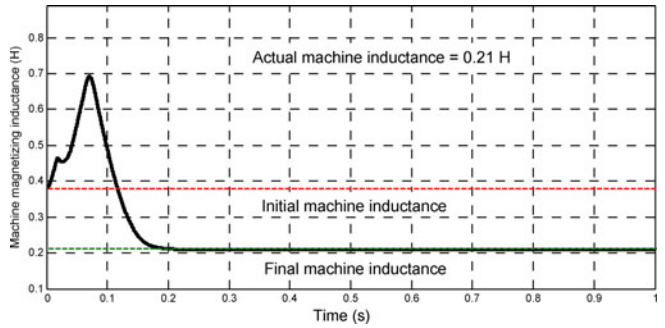

Fig. 27. Estimated mutual inductance of the machine during operation with a 100% error of the L_m at the start up (H).

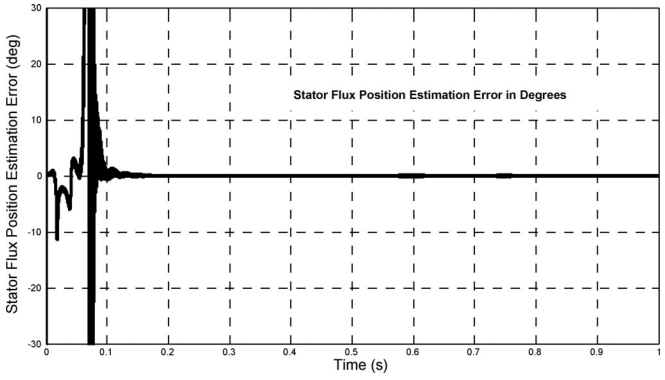

Fig. 28. Stator flux angle error during operation (in degrees).

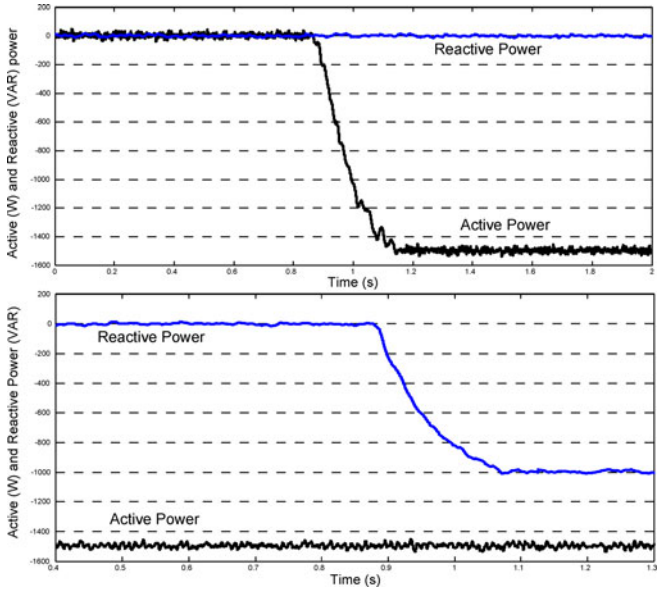

Fig. 29. Experimental results of the DDPC. Active and reactive power.

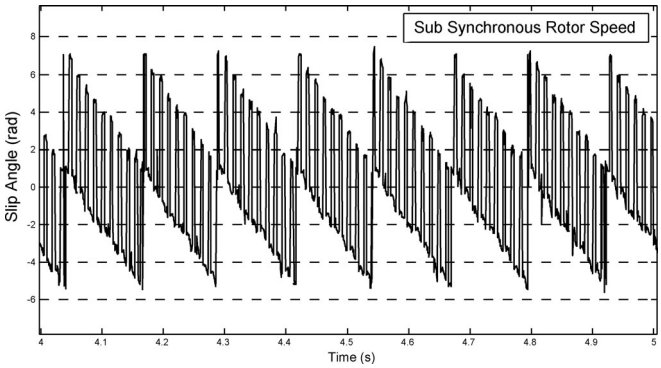

Fig. 30. Experimental results of estimated slip angle in subsynchronous rotor speed.

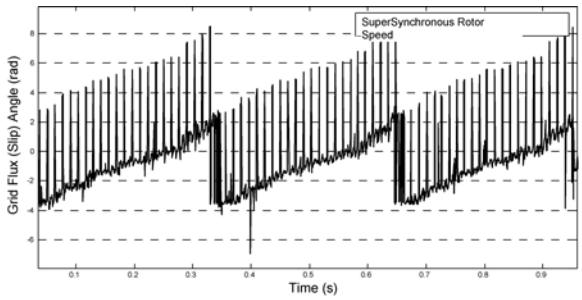

Fig. 31. Experimental results of estimated slip angle in supersynchronous rotor speed.

using the estimated mutual inductance is depicted. One can see from Fig. 28 that the estimation error of the stator flux angle reaches zero when the estimated L_m reaches its actual value in Fig. 27. In the following, the experimental results for the stator power output using the proposed power control are shown.

Fig. 29 shows that the proposed strategy can be used practically to control the power in a decoupled form, confirming the simulation results shown in Fig. 22. (Note that the longer power response time is due to mechanical limitations of the experimental setup and does not harm the main focus on the decoupling process.)

Figs. 30 and 31 show that the sensorless operation can accurately estimate the machine slip angle. Note that the spikes in Figs. 30 and 31 have a length of 2π rad and a frequency of 50 Hz.

VIII. Conclusion

In this paper, after analyzing the coupling between the active and reactive power control in the conventional DPC methods, an improved DDPC for the DFIM is proposed. Simulation and experimental results show the effectiveness of this method in decoupling the control loops of the stator active and reactive powers. Moreover, simulation and experimental results verify that the proposed method can accurately estimate the slip and rotor angles needed for the DPC control. The SVPWM controlled inverter of the rotor side maintains the switching frequency constant which reduces the power ripple. Furthermore, robustness to the variation of the machine mutual inductance *Lm* is achieved using a simple MRAS method.

References

[1] C. B. Mayer, "High response control of stator watts and vars for large wound rotor induction motor adjustable speed drives," *IEEE Trans. Ind. Appl.*, vol. IA-19, no. 5, pp. 736–743, Sep./Oct. 1983.

[2] R. Pena, J. C. Clare, and G. M. Asher, "Doubly fed induction generator using back-to-back PWM converter and is application to variable-speed wind-energy generation," *Proc. IEE B—Electr. Power Appl.*, vol. 143, no. 3, pp. 231–241, May 1996.

[3] J. Hu and Y. He, "Dynamic modeling and robust current control of wind turbine used DFIG during AC voltage dip," *J. Zhejiang Univ. Sci. A*, vol. 7, no. 10, pp. 1757–1764, Oct. 2006.

[4] S. Muller, M. Deicke, and R. W. De Doncker, "Doubly fed induction generator systems for wind turbines," *IEEE Trans. Ind. Appl.*, vol. 8, no. 3, pp. 26–33, May/Jun. 2002.

[5] J. Hu, Y. He, L. Xu, and B. W. Williams, "Improved control of DFIG systems during network unbalance using PI-R current regulators," *IEEE Trans. Ind. Electron.*, vol. 56, no. 2, pp. 439–451, Feb. 2009.

[6] I. Takahashi and T. Noguchi, "A new quick-response and high-efficiency control strategy of an induction motor," *IEEE Trans. Ind. Appl.*, vol. IA-22, no. 5, pp. 820–827, Sep. 1986.

[7] M. Depenbrock, "Direct self-control (DSC) of inverter-fed induction machine," *IEEE Trans. Power Electron.*, vol. 3, no. 4, pp. 420–429, Oct. 1988.

[8] G. S. Buja and M. P. Kazmierkowski, "Direct torque control of PWM inverter-fed ac motors: A survey," *IEEE Trans. Ind. Electron.*, vol. 51, no. 4, pp. 744–575, Aug. 2004.

[9] N. R. N. Idris and A. H. M. Yatim, "Direct torque control induction machines with constant switching frequency and reduced torque ripple," *IEEE Trans. Ind. Electron.*, vol. 51, no. 4, pp. 758–767, Aug. 2004.

[10] T. G. Habetler, F. Profumo, M. Pastorelli, and L. M. Tolbert, "Direct torque control of induction machines using space vector modulation," *IEEE Trans. Ind. Appl.*, vol. 28, no. 5, pp. 1045–1053, Sep. 1992.

[11] Y. S. Lai and J. H. Chen, "A new approach to direct torque control of induction motor drives for constant inverter switching frequency and torque ripple reduction," *IEEE Trans. Energy Convers.*, vol. 16, no. 3, pp. 220–227, Sep. 2001.

[12] R. Datta and V. T. Ranganathan, "Direct power control of grid-connected wound rotor induction machine without rotor position sensors," *IEEE Trans. Power Electron.*, vol. 16, no. 3, pp. 390–399, May 2001.

[13] L. Xu and P. Cartwright, "Direct active and reactive power control of DFIG for wind energy generation," *IEEE Trans. Energy Convers.*, vol. 21, no. 3, pp. 750–758, Sep. 2006.

[14] G. Abad, M. A. Rodriguez, and J. Poza, "Two-level VSC-based predictive torque control of the doubly fed induction machine with reduced torque and flux ripples at low constant switching frequency," *IEEE Trans. Power Electron.*, vol. 23, no. 3, pp. 1050–1061, May 2008.

[15] G. Abad, M. A. Rodriguez, and J. Poza, "Two-level VSC-based predictive direct power control of the doubly fed induction machine with reduced power ripple at low constant switching frequency," *IEEE Trans. Energy Convers.*, vol. 23, no. 2, pp. 570–580, Jun. 2008.

[16] D. Zhi and L. Xu, "Direct power control of DFIG with constant switching frequency and improved transient performance," *IEEE Trans. Energy Convers.*, vol. 22, no. 1, pp. 110–118, Mar. 2007.

[17] J. Hu, Y. He, and L. Xu, "Dynamic modeling and direct power control of wind turbine driven DFIG under unbalanced network voltage conditions," *J. Zhejiang Univ. Sci. A*, vol. 9, no. 12, pp. 1731–1740, Dec. 2008.

[18] J. Hu, H. Nian, B. Hu, Y. He, and Z. Q. Zhu, "Direct active and reactive power regulation of DFIG using sliding-mode control approach," *IEEE Trans. Energy Convers.*, vol. 25, no. 4, pp. 1028–1039, Dec. 2010.

[19] D. Zhi, L. Xu, and B. W. Williams, "Model-based predictive direct power control of doubly fed induction generators," *IEEE Trans. Power Electron.*, vol. 25, no. 2, pp. 341–351, Feb. 2010.

[20] G. Abad, M. A. Rodriguez, G. Iwanski, and J. Poza, "Direct power control of doubly- fed-induction-generator-based wind turbines under unbalanced grid voltage," *IEEE Trans. Power Electron.*, vol. 25, no. 2, pp. 442–452, Feb. 2010.

[21] N. Heng, S. Yipeng, P. Zhou, and Y. He, "Improved direct power control of a wind turbine driven doubly fed induction generator during transient grid voltage unbalance," *IEEE Trans. Energy Convers.*, vol. 26, no. 3, pp. 976–986, Aug. 2011.

[22] X. Hao, C. W. Zhang, and X. Zhang, "A comparison of sensorless control strategies of doubly fed induction generator," in *Proc. Int. Conf. Energy Environ. Technol.*, pp. 3–6.

[23] G. Abad, J. López, M. A. Rodríguez, L. Marroyo, and G. Iwanski, *Doubly Fed Induction Machine: Modeling and Control for Wind Energy Generation*. New York: Wiley, Sep. 2011.

[24] N. Amiri, S. M. Madani, and H. Abootorabi Zarchi, "Direct decoupled active and reactive power control of doubly fed induction machine without rotor position sensors and with robustness to saturation and parameter variation," in *Proc. Int. Electr. Mach. Drives Conf.*, May, 2011, pp. 747–752.

Navid Amiri (S'11) received the B.Sc. and M.Sc. degrees in electrical engineering in the field of power and electrical machines from the Isfahan University of Technology, Isfahan, Iran, in 2008 and 2011, respectively.

He is currently with the Isfahan University of Technology. His research interests include electrical machines and drives, electromechanical energy conversion, power electronics, and wind power generation systems.

Seyed M. Madani (S'97–M'03) received the B.Sc. degree from the Sharif University of Technology, Tehran, Iran, in 1989, the M.Sc. degree from the University of Tehran, Tehran, in 1991, and the Ph.D. degree from the Eindhoven University of Technology, Eindhoven, The Netherlands, in 1999, all in electrical power engineering.

From 2000 to 2003, he was an Associate Researcher in Texas A&M University. From 2003 to 2011, he worked at the University of Puerto Rico, University of Wisconsin at Madison, and Isfahan University of Technology as Assistant Professor. He is currently an Assistant Professor at the University of Isfahan, Isfahan, Iran.

His research interests include electrical machines, electric drives, and power electronics.

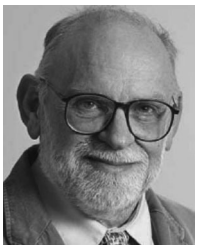

Thomas A. Lipo (M'64–SM'71–F'87–LF'04) was born in Milwaukee, WI. He received the B.E.E. and M.S.E.E. degrees from Marquette University, Milwaukee, in 1962 and 1964, respectively, and the Ph.D. degree in electrical engineering from the University of Wisconsin, Madison, in 1968.

From 1969 to 1979, he was an Electrical Engineer in the Power Electronics Laboratory of Corporate Research and Development of the General Electric Company, Schenectady, NY. He became a Professor of electrical engineering at Purdue University, West Lafayette, IN, in 1979. In 1981, he joined, as Professor, the University of Wisconsin–Madison, Madison, where he is currently the W.W. Grainger Professor for power electronics and electrical machines.

Dr. Lipo was the recipient of the Outstanding Achievement Award from the IEEE Industry Applications Society, the William E. Newell Award of the IEEE Power Electronics Society, and the 1995 Nicola Tesla IEEE Field Award from the IEEE Power Engineering Society. He has served the IEEE in various capacities, including the President of the Industry Applications Society. He is a Fellow of the Institution of Electrical Engineering, U.K., a member of the Institute of Electrical Engineering of Japan, a Fellow of the Royal Academy of Great Britain, and a Fellow of the National Academy of Engineering (U.S.).

Hossein Abootorabi Zarchi received the M.S. and Ph.D. degrees from the Isfahan University of Technology, Isfahan, Iran. He was a Visiting Ph.D. Student with the Control and Automation Group, Denmark Technical University, Denmark, from May 2009 to February 2010.

He is currently an Assistant Professor in the Department of Electrical Engineering, Ferdowsi University of Mashhad, Mashhad, Iran. His research interests include renewable energies, electrical machines, and applied nonlinear control in electrical drives.